Indonesian Journal of Electrical Engineering and Computer Science
Vol. 43, No. 2, August 2026, pp. 595~606
ISSN: 2502-4752, DOI: 10.11591/ijeecs.v43.i2.pp595-606

Affine-invariant feature learning for accurate ulcer detection in wireless capsule endoscopy images

S. Bhuvaneswari[1], M. Sulthan Ibrahim[2]
[1]Department of Computer Science, Madurai Kamaraj University, Madurai, India
[2]Department of Computer Science, Government Arts and Science College, Madurai, India

Article Info

Article history:

Received Sep 27, 2024
Revised May 28, 2026
Accepted Jul 23, 2026

Keywords:

Adaptive camarago's indexive
Affine invariant
Filtering technique
Regression
Ulcer detection
Vonneumannlocality
Wireless capsule endospcopy

ABSTRACT

Ulcers are lesions that develop in the lining of the gastrointestinal (GI) tract, particularly in the stomach and small intestine, and may lead to severe complications such as Crohn's disease and ulcerative colitis if not detected at an early stage. Conventional endoscopic procedures are often uncomfortable for patients and may provide limited visualization of the entire small intestine. Wireless capsule endoscopy (WCE) has emerged as a non-invasive alternative for comprehensive GI tract examination; however, automated ulcer detection from WCE images remains challenging due to image noise, complex tissue structures, and computational requirements. To address these issues, this paper proposes a Camargo's Indexive Kuwahara filtering-based affine-invariant sliced regression (CIKF-AISR) framework for accurate and efficient ulcer detection. The proposed framework consists of image acquisition, preprocessing, segmentation, and feature extraction stages. Adaptive CIKF is employed to suppress noise while preserving edge information. Subsequently, Von Neumann locality segmentation combined with the Canberra distance measure is utilized to identify regions of interest (ROIs). Finally, affine-invariant saliency sliced regression extracts discriminative shape, color, and texture features for ulcer detection. Experimental evaluation on the Hyper-Kvasir dataset demonstrates that the proposed method achieves higher ulcer detection accuracy, improved precision, enhanced peak signal-to-noise ratio (PSNR), and lower detection time compared with existing deep CNN and VAE-GAN approaches. These results confirm the effectiveness of the proposed framework for computer-aided GI diagnosis.

This is an open access article under the CC BY-SA license.

Corresponding Author:

S. Bhuvaneswari
Department of Computer Science, Madurai Kamaraj University
Madurai, India
Email: bhuvaeswari.s@cpacollege.org

1. INTRODUCTION

Gastrointestinal (GI) diseases are among the most prevalent health disorders worldwide and continue to pose significant challenges to healthcare systems. Among these disorders, ulcers are common lesions that develop in the lining of the stomach, small intestine, or other regions of the GI tract. If left untreated, ulcers may progress to severe complications, including GI bleeding, Crohn's disease, and ulcerative colitis. Consequently, early and accurate ulcer detection is essential for timely clinical intervention and effective disease management.

Recent advances in medical imaging technologies have substantially improved the diagnosis of GI disorders. Among the available diagnostic modalities, wireless capsule endoscopy (WCE) has emerged as a

valuable and minimally invasive technique for visualizing the entire GI tract, particularly regions that are difficult to access using conventional endoscopy. WCE systems capture thousands of high-resolution images during a single examination, providing comprehensive information for detecting ulcers and other GI abnormalities. However, the large volume of generated images makes manual examination labor-intensive, time-consuming, and susceptible to observer variability. As a result, automated ulcer detection systems based on machine learning (ML) and deep learning (DL) have received considerable attention from researchers.

Several studies have explored ML- and DL-based approaches for ulcer detection and GI disease diagnosis. Deep convolutional neural networks (CNNs) were employed in [1] to enhance the visibility of WCE images and improve ulcer detection performance. Although improved contrast and edge representation were achieved, image noise amplification remained a challenge. An integrated variational autoencoder-generative adversarial network (VAE-GAN) framework was proposed in [2] for ulcer detection; however, accurate segmentation of regions of interest (ROIs) remained difficult. CNN-based models were also introduced for ulcer and erosion classification in capsule endoscopy images [3], while DL approaches for endoscopic image categorization were investigated in [4]. Hybrid architectures such as CNN-FFNN and CNN–XGBoost were developed in [5] for GI disease diagnosis, but they exhibited limitations in achieving high accuracy with low computational cost. Similarly, three-dimensional CNNs [6], ML algorithms for capsule endoscopy image categorization [7], and fully automated DL frameworks [8] demonstrated promising performance but suffered from issues related to computational complexity, segmentation accuracy, or feature utilization.

Additional studies have investigated automated GI disease detection using multi-method systems [9], multi-branch CNN architectures [10], and CNN-based disease classification models [11]. DL frameworks such as ResNet50 [12], artificial intelligence-based prediction systems [13], and class-balanced high-resolution networks [14] have also been explored for ulcerative colitis assessment and related GI disorders. Furthermore, multicenter deep learning models for endoscopic severity grading [15], automated disease activity assessment [16], hybrid feature fusion frameworks [17], Mayo endoscopic score prediction models [18], [19], deep neural network-based endoscopic evaluation [20], interpretable deep learning approaches for inflammatory bowel disease classification [21], computer vision systems for endoscopic disease quantification [22], neural network-based central reading systems [23], and several deep CNN and pathology-sensitive architectures for gastrointestinal abnormality detection [24]–[30] have been proposed. Despite their encouraging results, many of these approaches require extensive computational resources, rely heavily on large annotated datasets, or exhibit limitations in image enhancement, ROI extraction, and efficient feature representation.

A careful analysis of the existing literature reveals several important research challenges. First, WCE images are often affected by noise and illumination variations that degrade image quality and reduce diagnostic reliability. Second, many existing approaches focus primarily on classification performance while overlooking robust preprocessing mechanisms that preserve diagnostically significant image structures. Third, inaccurate segmentation of ulcer-related regions may introduce irrelevant information into the analysis process, thereby increasing computational complexity and reducing detection performance. Finally, DL-based methods often require substantial computational resources and large training datasets, limiting their applicability in practical clinical environments.

Motivated by these limitations, this paper proposes a Camargo's Indexive Kuwahara filtering-based affine-invariant sliced regression (CIKF-AISR) framework for ulcer detection using WCE images. The proposed framework integrates adaptive image preprocessing, efficient ROI extraction, and discriminative feature analysis within a unified detection pipeline. Initially, adaptive CIKF is employed to suppress noise while preserving edge information and improving image quality. Subsequently, Von Neumann locality segmentation combined with the Canberra distance measure is utilized to accurately identify and extract ulcer-related ROIs. Finally, affine-invariant saliency sliced regression is applied to extract significant shape, color, and texture features that facilitate accurate ulcer detection. Through the integration of these components, the proposed CIKF-AISR framework aims to improve peak signal-to-noise ratio (PSNR), enhance ulcer detection accuracy and precision, and reduce computational time compared with existing approaches. Experimental evaluations conducted on the Hyper-Kvasir dataset demonstrate the effectiveness of the proposed method for computer-aided GI disease diagnosis.

2. PROPOSED METHOD

Ulcer diseases are a major health concern, affecting many people's worldwide. These are characterized by lesions that develop on the inside layer of stomach, small intestine, or other areas of the GI area. A common symptom of ulcer diseases includes an abdominal pain, indigestion, nausea, and vomiting. Detecting ulcer diseases at an early stage is crucial for effective management and treatment. Ulcer detection improved using WCE images of GI tract. CIKF-AISR developed. It captures GI tract images to visualize an apparent view of its internal parts of the human body than the conventional endoscopy techniques. WCE also

offers a less persistent and more comfortable alternative for patients than the traditional endoscopy. The small capsule, which contains miniature camera, has ingested via patient as well as transmits images because it passes during digestive system. Conventionally, ulcer detection using machine as well asDL algorithms has been developed in early detection and treatment. However, achieving accurate ulcer detection with lesser time complexity faces major challenges. CIKF-AISR method for improving the ulcer detection accuracy with minimal time and higher peak to signal to noise ratio.

Architecture diagram of proposed CIKF-AISR technique for accurate detection of ulcer detection with WCE images demonstrated in Figure 1. The proposed ulcer detection method involves four fundamental steps namely image acquisition, preprocessing, segmentation and feature extraction. These fundamental processes of the proposed CIKF-AISR technique are explained briefly in the following subsections.

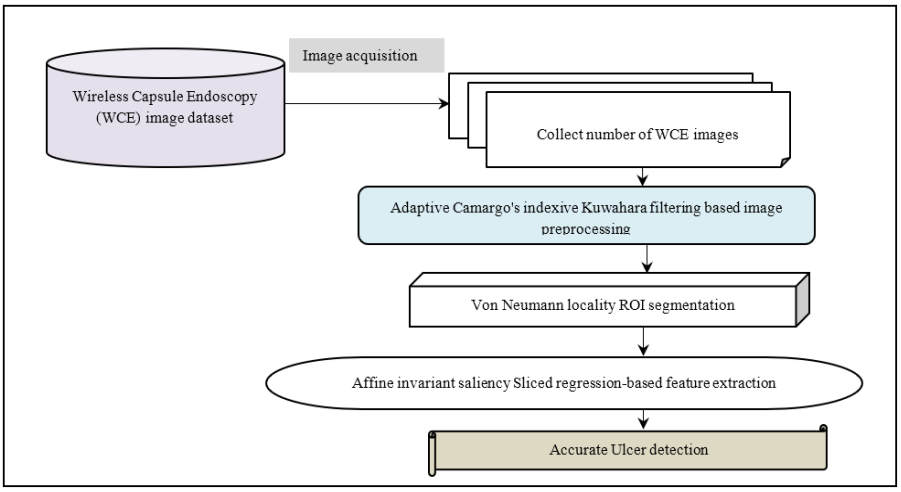

Figure 1. Block diagram of proposed CIKF-AISR

2.1. image acquisition

It has procedure of collecting the WCE image as ofHyper-Kvasir dataset. It has widely unconfined GI tract image dataset for ulcer detection. It hasseparatedto four separate elements such as Labeled image data, unlabeled image data, segmented image data, as well as annotated video data. Amongst these parts, labeled images employed to estimate experimental. From the labeled images, ulcer WCE images gathered to find disease.

2.2. preprocessing

Preprocessing is a fundamental step to achieve higher WCE image quality for further analysis. Proposed technique utilizes adaptive CIKF for image denoising to improve image quality. CIKF is a non-linear smoothing filter used for adaptive noise reduction in WCE images. Proposed filter is able to apply smoothing on WCE images while preserving the edges also.

Figure 2 illustrates block diagram of adaptive CIKF for image noise artifacts removal in given WCE image. Let us consider number of inputs WCE image denoted as $EI_1, EI_2, EI_3, \dots, EI_n$ taken from dataset. For each input images, pixels are extracted and it represented by$P_1, P_2, P_3, \dots, P_m$. Pixels areorganized by filtering window size. It measured as,

$$R = 2 * k + 1 \quad (1)$$

where, filtering window size denoted as R, k denotes a radius of filter. Thefour square quadrants with size $(+1) * (k + 1)$ is used to arrange the pixels in the form of row 'i' and column 'j'where, $(1 \leq i \leq h)$ and, $(1 \leq j \leq w)$.

First, numbers of pixels aredivided into four square quadrants as given below,

$$q_m = P\,[(i - k, i + k) * (j - k, j + k)] \quad (2)$$

where, q_m denotes a square quadrant, input pixels of images 'P' partitioned four square quadrants such as $i - k, i + k, j - k$, and $j + k$ respectively.

These four-square quadrants are expressed as follows,

$$q_1 = P(i-k, i) * (j-k, j) \quad (3)$$

$$q_2 = P(i-k, i) * (j, j+k) \quad (4)$$

$$q_3 = P(i, i+k) * (j-k, j) \quad (5)$$

$$q_4 = P(i, i+k) * (j, j+k) \quad (6)$$

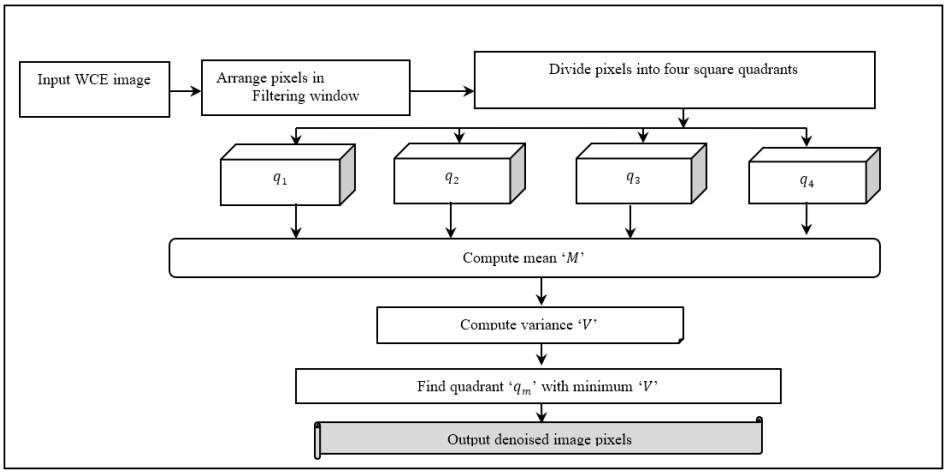

Figure 2. Flow process of adaptive Camargo's indexive Kuwahara filtering technique

The layout of a $5 * 5$ Kuwahara kernel with four square quadrants is shown below.

Figure 3 illustrates the pixel arrangement or layout of in $5 * 5$ Kuwahara kernel window. At ascending order, pixels positioned. Filtering window is partitioned into four quadrants q_1, q_2, q_3, and q_4. As shown in Figure 3, CP indicates center pixels of kernel window

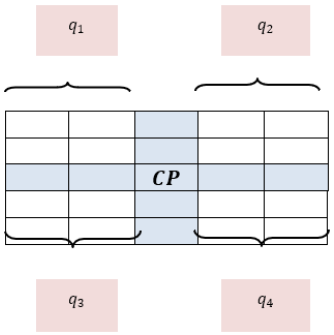

Figure 3. Layout of a $5 * 5$ Kuwahara filter kernel

For each quadrant q, the mean (M) and deviation (M) is calculated. Then compute the mean for each quadrant is computed as follows,

$$M(q) = \frac{1}{n\,(q)} \sum_{i=1}^{h} \sum_{j=1}^{w} Pv_{ij} \quad (7)$$

where, $M(q)$ denotes a mean of pixels, $\sum_{i=1}^{h} \sum_{j=1}^{w} Pv_{ij}$ denotes a sum of all the pixel value in the particular quadrant, number of pixels denoted as $n\,(q)$ at particular quadrant. Center pixels 'CP' is computed depended on mean value follows,

$$CP = \frac{1}{4}\sum_{t=1}^{4} M_t(q) \quad (8)$$

where, $M_t(q)$ denotes a mean of all four quadrants. After that, the deviation is computed for each quadrant based on the above estimated mean value by applying a Camargo's index. The Camargo's index is a qualitative method to measure the dependency between pixel values and the mean of particular quadrant. The Camargo's index function is formulated as follows,

$$CI(q) = 1 - \sum_{i=1}^{h}\sum_{j=1}^{w} \frac{|Pv_{ij} - M(q)|}{n\,(q)} \quad (9)$$

where, $CI(q)$ indicates an output Camargo's index function for particular quadrant, Pv_{ij} denotes a pixel value in the particular quadrant, $M(q)$ indicates mean of pixels in the particular quadrant, $n\,(q)$ indicates a number of pixels. From the analysis, the index function provides the output ranges from the 0 to 1. After that, minimum deviation among the four quadrants is identifiedthrough higher output ranges of Camargo's index function.

$$Y = \begin{cases} min\,dev\ , & CI(q) > T \\ max\,dev, & CI(q) < T \end{cases} \quad (10)$$

Where, Y denotes a filtered output, $\min dev$ denotes a minimum deviation, $\max dev$ denotes a maximum deviation T denotes a threshold, $CI(q)$ indicates a output Camargo's index function. From the analysis, the pixels with minimum deviation from the mean pixels are called normal pixels. Otherwise, the pixels with maximum deviation from the mean are called noise pixels. The noise pixels are then removed from the filtering window through replacing average of normal pixels within respective quadrant. This denoising process effectively reduces MSE as well asenhances PSNR resulting in enhanced image quality.

Algorithm 1 describes the various steps involved in enhancing image quality by filtering out noise pixels. Finally, the quality-enhanced image is obtained with lesser MSE as well as higher PSNR.

Algorithm 1. Adaptive Camargo's indexive Kuwahara filtering technique

```
Input: image database, Number of input WCE image EI_1, EI_2, EI_3, .... EI_n
Output:  Preprocessed images
Begin
Step 1:  Collect number of input WCE image EI_1, EI_2, EI_3, .... EI_n from datast
Step 2:    For each input image EI_i
Step 3:       Extract the number of pixels  P_1, P_2, P_3, .... P_m
Step 4:       Organize the pixels in filtering window in ascending order
Step 5:   Divide the image pixels into four quadrants using (3) (4) (5) (6)
Step 6:        For each quadrant q
Step 7:              Compute mean using (7)
Step 8:              Define center pixel value 'CP' using (8)
Step 9:           Compute the deviation using Camargo's index (9)
Step 10:      if(CI(q) > T)  then
Step 11:           Returns minimum deviation between the pixels and mean
Step 12:         else
Step 13:  Returns maximum deviation between the pixels and mean
Step 14:  end if
Step 15:     Select minimum deviation pixels and remove maximum deviation pixels
Step 16:     Replace noisy pixels with mean value of normal pixel
Step 17: End for
Step 18: End for
Step 19: Return (quality enhanced image)
End
```

2.3. Von Neumann locality Image segmentation

After the image preprocessing, the CIKF-AISR technique performs the segmentation to partition image to several segments depended on certain pixel intensity characteristics. The CIKF-AISR technique utilizes the Von Neumann locality segmentation method is employed to segment the image into different regions and extract the ROI with Canberra distance measure between the image pixels. The Von Neumann locality segmentation is a concept used in image processing to define set of spatial relationship between a set of neighboring pixels. It defines the connectivity of pixels in image processing tasks. This locality segmentation is used to define the notion of 4-connected pixels surrounding a central pixel.

Figure 4 depicts a 4-connected neighborhood pixels method or Von Neumann pixels connectivity. First, the starting point is marked with a central pixel located in two-dimensional space ($P_{x,y}$). The neighborhood connectivity is measured using Canberra distance measure between the pixels.

	$P_{x,y-1}$	
$P_{x-1,y}$	$P_{x,y}$	$P_{x+1,y}$
	$P_{x,y+1}$	

Figure 4. Von Neumann pixels connectivity

$$S = arg\,min\{CD(P_{x,y}, P_{NN})\} \tag{11}$$

$$P_{NN} = \begin{Bmatrix} P_{x-1,y} \\ P_{x+1,y} \\ P_{x,y-1} \\ P_{x,y+1} \end{Bmatrix} \tag{12}$$

$$CD(P_{x,y}, P_{NN}) = \frac{(P_{x,y} - P_{NN})}{|P_{x,y}| + |P_{NN}|} \tag{13}$$

Where, 'S' denotes a connectivity between the pixel intensity, $\arg min$ denotes a argument of minimum function, CD denotes a Canberra distance between the two pixels $P_{x,y}$ and P_{NN}, $P_{x,y}$ denotes a center pixels intensity, P_{NN} denotes four another pixel's intensity, $|P_{x,y}|$ denotes absolute value of center pixels intensity, $|P_{x,y}|$ denotes absolute value of another pixel's intensity. Therefore, the minimum distance between pixel intensities is considered adjacency or neighborhood, facilitating the connection of similar regions. This approach is utilized in image segmentation, where regions with similar pixel intensities are grouped together. Subsequently, ROIs, such as infected regions are extracted for ulcer detection. This process helps minimize time complexity of ulcer detection for considering ROIs in image.

Algorithm 2 outlines the steps involved in image segmentation to minimize the time complexity of ulcer detection. Finally, the segmented images are obtained to improve the process of ulcer detection with minimal time.

Algorithm 2. Von Neumann locality image segmentation

```
Input: Number of preprocessed images EI_1, EI_2, EI_3, …., EI_n
Output: Segmented image
Begin
Step 1:  Collect the preprocessed images EI_1, EI_2, EI_3, …., EI_n,
Step 2:for every input image
Step 3:Measure the degree of connectivity between the pixels using (11)
Step 4:    if arg min{CD(P_x,y, P_NN )}then
Step 5:          Find Adjacent pixels
Step 6:   end if
Step 7:end for
Step 8:  Segment the ROI from image
End
```

2.3.1. Affine invariant saliency Sliced regression method-based feature extraction

In order to improve ulcer detection accuracy, affine invariant saliency sliced regressionperforms feature extraction. Sliced inverse regression is a ML technique for dimensionality reduction in multivariate statistics. The dimensionality reduction is the process used to reduce the representation of an image by extracting the significant features like, shape, color, and textures.

$$Z = (\omega_1{}^T F_1,\ \omega_2{}^T F_2, \omega_3{}^T F_3,\ \varepsilon) \tag{14}$$

where, Z denotes a regression outcome, $\omega_1, \omega_2, \omega_3$ are projection vectors to extract the three features namely shape, T denotes a transpose, 'F_1' indicates ashapefeature, 'F_2'indicaes a color feature, and texture feature 'F_3', the symbol ε represents the error term. It represents the difference between the observed value and the value obtained by the regression model.

The Affine invariant saliency refers to a measure of the importance of image regions that remains consistent under affine transformations. To detect affine-invariant regions, an ellipse detection approach is employed for shape detection. This approach parameterizes regions using three parameters namely scale (α), axis ratio (β), and orientation (θ).

The scale parameter represents the size of the ellipse or image regions. It is defined as the average distance between the center and its boundary. Let us consider the center co-ordinates of object points (u_1, v_1), and the boundary co-ordinates of objects (u_2, v_2). The distance is computed from the center and the boundary as given below,

$$ED = \sqrt{(u_2 - u_1)^2 + (v_2 - v_1)^2} \tag{15}$$

based on the distance measure 'ED', the closed contour is determined, which helps in identifying the shape within the image.

The axis ratio parameter represents the ratio of the lengths of the major and minor axes. It is expressed as follows,

$$\beta = \frac{a}{b} \tag{16}$$

where, a denotes a major axis, b indicates a minor axis.

Orientation (θ) parameter represents the rotation angle of the ellipse relative to the x-axis.

$$\theta = tan^{-1}\left(\frac{(u_2 - u_1)}{(v_2 - v_1)}\right) \tag{17}$$

Where, (u_1, v_1) denotes a center co-ordinate of points, and (u_2, v_2) denotes a boundary co-ordinate point.

Quantized color histograms is employed for distribution of pixel intensities. In the first step is to convert the image from its original color space RGB (red, Green, blue) to a suitable color space HSV (Hue (C_H), Saturation (C_S), and Value (C_V)). The color conversion process is given below,

$$C_H = cos^{-1}\left[\frac{1}{2} * \frac{[(R-G)+(R-B)]}{\sqrt{(R-G)^2+(R-G)(G-B)}}\right] \tag{18}$$

$$C_S = 1 - 3 * \frac{1}{(R+G+B)}[argmin(R, G, B)] \tag{19}$$

$$C_V = \frac{1}{3} * [(R + G + B)] \tag{20}$$

Once the image is in the desired color space, a histogram is computed for each color channel. A histogram is a representation of the frequency of occurrence of different color values within a specified range. If the color space is large, then it first divides into certain numbers of smaller intervals. Each of the intervals is called a bin. This process is called color quantization. After the quantization, the histogram is computed as follows,

$$r_i = b_1 \cup b_2 \cup b_3 \ldots\ldots \cup b_k \tag{21}$$

Where, r_i size of input color space, $b_1, b_2 \ldots b_n$ denotes a bins, ∪ denotes a union symbol. After that, the histogram is computed for each bin is given below,

$$H(k) = count(P_i\ (b_k)) \tag{22}$$

where, $H(k)$ represents the histogram i.e., frequency of occurrence of pixels in k^{th} bin, $count(P_i\ (b_k))$ denotes counts the number of pixels in the image that have an intensity value falling within the bin b_k of the histogram. In this way, the color histogram of the image is obtained.

Texture feature is used to provide the spatial correlation between the pixels' intensities within the ROI image.

$$Tf = \frac{1}{v_i * v_j}\sum_i \sum_j (P_i - \mu_i)(P_j - \mu_j) \tag{23}$$

where 'Tf' indicates the texture feature, P_i denotes a pixel, P_j denotes a neighboring pixel, μ_i and μ_j indicates a mean of the pixels and neighboring pixels, v_i and v_j indicates a deviation of the pixels and neighboring pixels.

Algorithm 3, outlines feature extraction process for enhancing the accuracy of ulcer detection. Resulting features subsequently utilized to enhance the accuracy of ulcer detection.

Algorithm 3. Feature extraction

```
Input: segmented images ROI
Output: extract the features
Begin
Step 1:  for each segmented image
Step 2:  Apply regression to project the feature vector using (14)
Step 3:     Extract the shape features using (15) (16) (17)
Step 4:   Convert RGB into HSV using (18) (19) (20)
Step 5:     Divide color space into bin using r_i = b_1 ∪ b_2 ∪ b_3 …..∪ b_k
Step 6:     Measure color histogram (22)
Step 7:      Extract texture feature using correlation using (23)
Step 8:  end for
Step 9:  Extract significant features
End
```

3. EXPERIMENTAL SETUP

The proposed CIKF-AISR technique is implemented using MATLAB and evaluated against two existing ulcer detection methods, namely deep CNN [1] and VAE-GAN [2]. All experiments are conducted under the same implementation environment to ensure a fair comparison among the competing approaches. To evaluate the performance of the proposed framework, the Hyper-Kvasir dataset is employed. Hyper-Kvasir is one of the largest publicly available GI image datasets and contains 110,079 images and 373 videos representing anatomical landmarks, pathological findings, therapeutic interventions, and normal GI conditions. The dataset is divided into several categories, including labeled images, unlabeled images, segmented images, and annotated videos. In this study, only the labeled WCE images corresponding to ulcer cases are utilized for experimental evaluation.

Among the available labeled samples, a total of 851 ulcer images are collected and used for analysis. To investigate the scalability and robustness of the proposed method, different subsets ranging from 50 to 500 images are selected from the dataset. Prior to feature extraction and ulcer detection, all input images undergo preprocessing using the proposed adaptive CIKF technique to reduce noise and preserve diagnostically relevant edge information. Subsequently, Von Neumann locality segmentation is applied to identify and extract ulcer-related ROIs from the preprocessed images.

The extracted ROIs are then processed using the proposed affine-invariant saliency sliced regression framework to obtain discriminative shape, color, and texture features. These features are subsequently employed for ulcer detection and performance evaluation. The effectiveness of the proposed CIKF-AISR framework is assessed using several quantitative metrics, including PSNR, ulcer detection accuracy, precision, and ulcer detection time. PSNR is used to evaluate the quality of the preprocessed images, while accuracy and precision measure the effectiveness of ulcer identification. Detection time is employed to assess the computational efficiency of the proposed method.

For comparative analysis, the same dataset partitions and evaluation conditions are applied to the deep CNN [1] and VAE-GAN [2] approaches. The experimental results obtained from these methods are compared with those of the proposed CIKF-AISR framework to demonstrate its effectiveness in improving image quality, enhancing ulcer detection performance, and reducing computational complexity in WCE image analysis.

4. COMPARATIVE PERFORMANCE ANALYSIS

CIKF-AISRtechnique, along with two existing methods, deep CNN [1] VAE-GAN [2] compared. The performance analysis employs different metrics. Performance of each technique in terms of these metrics is illustrated through tables and graphical representations.

4.1. performance analysis of Peak signal to noise ratio

Quality of preprocessed WCE image measured as PSNR, by comparing it to the original image. SNR determined to compute MSEamong original as well as preprocessed WCE image.

$$PSNR = 10 * log_{10}\left[\frac{{P_{mx}}^2}{E_{MS}}\right] \quad (24)$$

$$E_{MS} = [O_{size} - Pr_{size}]^2 \quad (25)$$

where peak signal to noise ratio is '$PSNR$', 'P_{mx}' represents maximum possible pixel value (255), E_{MS} indicates a mean square error, Pr_{size} indicates preprocessed image size, O_{size} denotes original image

size. It is expressed in decibels (dB). Three methods namely CIKF-AISR technique, deep CNN [1] VAE-GAN [2] are employed in Table 1. The average of ten comparisons results shows that PSNR was enhanced using CIKF-AISR technique by 17% and 8% when compared to [1] [2].

Table 1. PSNR

WCE image size (KB)	PSNR (dB)		
	CIKF-AISR	deep CNN	VAE-GAN
228	54.15	46.54	50.06
214.7	62.11	51.22	56.08
171.3	58.58	49.04	54.15
270.4	62.11	56.08	58.58
233	60.17	52.86	57.50
235.3	63.27	55.87	59.18
244.7	57.50	51.22	54.15
191.8	64.60	50.06	55.26
266.8	60.89	53.16	57.24
267.4	63.52	55.06	58.58

4.2. Performance analysis of ulcer detection accuracy

It measured as number of WCE images accurately detected. Accuracy mathematically formulated as given below,

$$UDA = \left(\frac{TR_p+TR_n}{TR_p+TR_n+FL_p+FL_n}\right) * 100 \quad (26)$$

where, UDA indicates ulcer detection accuracy, TR_p denotes the true positives, true negative is TR_n, false positive is FL_p, false negative FL_n indicates false negative. The accuracy is measured in percentage (%).

Figure 5 demonstrates a performance analysis of ulcer detection accuracy versus the number of WCE images. The overall comparison results prove that the CIKF-AISR technique increased accuracy by 9% and 5% than the [1], [2].

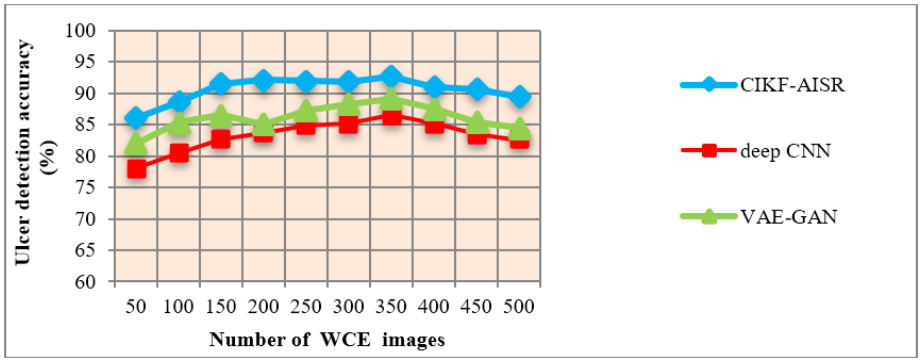

Figure 5. performance results of ulcer detection accuracy

4.3. Performance analysis of precision

It is the measures of ratio of true positive detection of ulcer disease made by the model. Precision computed by,

$$Pre = \frac{TR_p}{TR_p+FL_p} \quad (27)$$

where, Pre denotes a precision, TR_p denotes a true positive that the images are correctly detected as ulcer, FL_p indicates a false positive refer to images incorrectly detected as ulcer. Table 2 illustrates a performance analysis of precision in ulcer detection. On average, the comparison of ten results reveals that the precision performance during ulcer detection was increased by 9% compared to deep CNN [1] and by 5% compared to VAE-GAN [2].

Table 2. Precision versus number of WCE images

Number of WCE images	Precision (%)		
	CIKF-AISR	Deep CNN	VAE-GAN
50	0.902	0.837	0.871
100	0.912	0.845	0.875
150	0.915	0.832	0.856
200	0.908	0.855	0.866
250	0.911	0.826	0.857
300	0.895	0.835	0.858
350	0.918	0.847	0.869
400	0.907	0.833	0.875
450	0.905	0.826	0.855
500	0.903	0.818	0.852

4.4. Performance analysis of ulcer detection time

The overall time for ulcer detection from the given input WCE images is measured as the amount of time the algorithm's taken to detect the ulcers. It is mathematically calculated as follows,

$$UDT = \sum_{i=1}^{n} EI_i * Tme\ [UD] \quad (28)$$

where, UDT indicates the ulcer detection time, $Tme[UD]$ indicates a time for detection of single image 'EI_i'. The overall time estimated in milliseconds (ms).

Figure 6 illustrates performance analysis of ulcer detection timeusing CIKF-AISR and deep CNN [1], VAE-GAN [2]. From this analysis, the ulcer detection timeusing CIKF-AISR technique was minimized by 15% and 8% than the [1] and [2].

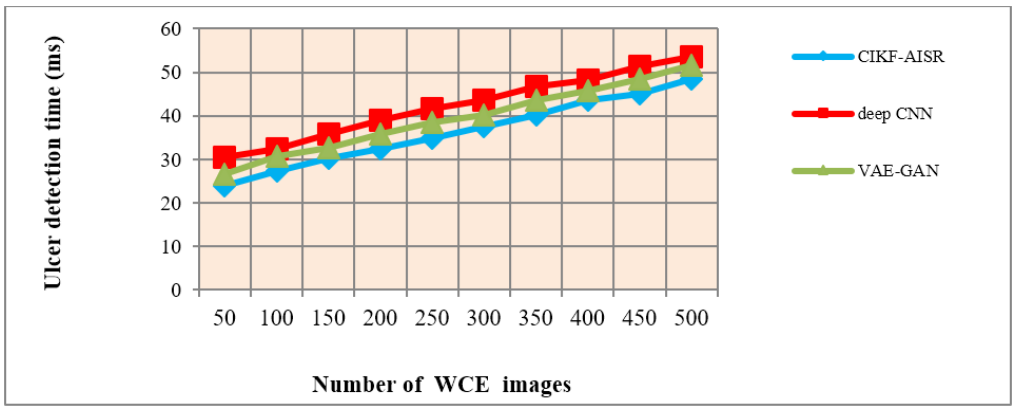

Figure 6. Performance results of ulcer detection time

5. CONCLUSION

This paper presented a CIKF-AISR framework for automated ulcer detection using WCE images. The proposed framework integrates adaptive image preprocessing, region-of-interest segmentation, and affine-invariant feature extraction to improve ulcer detection performance while reducing computational complexity. Adaptive CIKF was employed to suppress noise and preserve edge information, thereby enhancing image quality. Subsequently, Von Neumann locality segmentation combined with the Canberra distance measure was utilized to accurately extract ulcer-related ROIs. Finally, affine-invariant saliency sliced regression was applied to derive discriminative shape, color, and texture features for ulcer identification. Experimental evaluations conducted on the Hyper-Kvasir dataset demonstrated the effectiveness of the proposed framework. Comparative results showed that CIKF-AISR achieved superior ulcer detection accuracy, higher precision, improved PSNR, and reduced detection time compared with deep CNN and VAE-GAN approaches. These improvements indicate that the proposed framework can effectively enhance diagnostic reliability while maintaining computational efficiency for large-scale WCE image analysis. The obtained results demonstrate the potential of CIKF-AISR as a computer-aided diagnostic tool for GI ulcer detection. Future work may focus on integrating advanced DL architectures and validating the framework on larger multicenter datasets to further improve its robustness and clinical applicability.

REFERENCES

[1] V. V and K. V. M. Prashanth, "Ulcer detection in wireless capsule endoscopy images using deep CNN," *Journal of King Saud University - Computer and Information Sciences*, vol. 34, no. 6, pp. 3319–3331, Jun. 2022, doi: 10.1016/j.jksuci.2020.09.008.

[2] D. Bajhaiya, S. N. Unni, and A. K. Koushik, "Deep learning–powered generation of artificial endoscopic images of GI tract ulcers," *iGIE*, vol. 2, no. 4, pp. 452-463.e2, Dec. 2023, doi: 10.1016/j.igie.2023.08.002.

[3] J. Afonso *et al.*, "Development of a convolutional neural network for detection of erosions and ulcers with distinct bleeding potential in capsule endoscopy," *Techniques and Innovations in Gastrointestinal Endoscopy*, vol. 23, no. 4, pp. 291–296, 2021, doi: 10.1016/j.tige.2021.06.003.

[4] H. H. Yen *et al.*, "Performance comparison of the deep learning and the human endoscopist for bleeding peptic ulcer disease," *Journal of Medical and Biological Engineering*, vol. 41, no. 4, pp. 504–513, Aug. 2021, doi: 10.1007/s40846-021-00608-0.

[5] I. A. Ahmed, E. M. Senan, and H. S. A. Shatnawi, "Hybrid models for endoscopy image analysis for early detection of gastrointestinal diseases based on fused features," *Diagnostics*, vol. 13, no. 10, p. 1758, May 2023, doi: 10.3390/diagnostics13101758.

[6] M. Bordbar, M. S. Helfroush, H. Danyali, and F. Ejtehadi, "Wireless capsule endoscopy multiclass classification using three-dimensional deep convolutional neural network model," *BioMedical Engineering Online*, vol. 22, no. 1, p. 124, Dec. 2023, doi: 10.1186/s12938-023-01186-9.

[7] T. Kratter *et al.*, "Deep learning multi-domain model provides accurate detection and grading of mucosal ulcers in different capsule endoscopy types," *Diagnostics*, vol. 12, no. 10, p. 2490, Oct. 2022, doi: 10.3390/diagnostics12102490.

[8] M. A. Khan *et al.*, "Computer-aided gastrointestinal diseases analysis from wireless capsule endoscopy: a framework of best features selection," *IEEE Access*, vol. 8, pp. 132850–132859, 2020, doi: 10.1109/ACCESS.2020.3010448.

[9] S. M. Fati, E. M. Senan, and A. T. Azar, "Hybrid and deep learning approach for early diagnosis of lower gastrointestinal diseases," *Sensors*, vol. 22, no. 11, p. 4079, May 2022, doi: 10.3390/s22114079.

[10] M. Martins *et al.*, "Deep-learning and device-assisted enteroscopy: automatic panendoscopic detection of ulcers and erosions," *Medicina (Lithuania)*, vol. 59, no. 1, p. 172, Jan. 2023, doi: 10.3390/medicina59010172.

[11] J. Yogapriya, V. Chandran, M. G. Sumithra, P. Anitha, P. Jenopaul, and C. S. G. Dhas, "Gastrointestinal tract disease classification from wireless endoscopy images using pretrained deep learning model," *Computational and Mathematical Methods in Medicine*, vol. 2021, pp. 1–12, Sep. 2021, doi: 10.1155/2021/5940433.

[12] N. Higuchi *et al.*, "Automated evaluation of colon capsule endoscopic severity of ulcerative colitis using ResNet50," *PLoS ONE*, vol. 17, no. 6 June, p. e0269728, Jun. 2022, doi: 10.1371/journal.pone.0269728.

[13] P. Biamonte *et al.*, "New Technologies in Digestive Endoscopy for Ulcerative Colitis Patients," *Biomedicines*, vol. 11, no. 8, p. 2139, Jul. 2023, doi: 10.3390/biomedicines11082139.

[14] G. Wang *et al.*, "CB-HRNet: A Class-Balanced High-Resolution Network for the evaluation of endoscopic activity in patients with ulcerative colitis," *Clinical and Translational Science*, vol. 16, no. 8, pp. 1421–1430, Aug. 2023, doi: 10.1111/cts.13542.

[15] R. T. Sutton, O. R. Zaïane, R. Goebel, and D. C. Baumgart, "Artificial intelligence enabled automated diagnosis and grading of ulcerative colitis endoscopy images," *Scientific Reports*, vol. 12, no. 1, p. 2748, Feb. 2022, doi: 10.1038/s41598-022-06726-2.

[16] B. Gutierrez Becker *et al.*, "Training and deploying a deep learning model for endoscopic severity grading in ulcerative colitis using multicenter clinical trial data," *Therapeutic Advances in Gastrointestinal Endoscopy*, vol. 14, Jan. 2021, doi: 10.1177/2631774521990623.

[17] H. Yao *et al.*, "Fully automated endoscopic disease activity assessment in ulcerative colitis," *Gastrointestinal Endoscopy*, vol. 93, no. 3, pp. 728-736.e1, Mar. 2021, doi: 10.1016/j.gie.2020.08.011.

[18] J. Qi *et al.*, "PHF3 technique: a pyramid hybrid feature fusion framework for severity classification of ulcerative colitis using endoscopic images," *Bioengineering*, vol. 9, no. 11, p. 632, Nov. 2022, doi: 10.3390/bioengineering9110632.

[19] J. E. Kim *et al.*, "Deep learning model for distinguishing Mayo endoscopic subscore 0 and 1 in patients with ulcerative colitis," *Scientific Reports*, vol. 13, no. 1, p. 11351, Jul. 2023, doi: 10.1038/s41598-023-38206-6.

[20] J. Qi *et al.*, "Development and validation of a deep learning-based approach to predict the Mayo endoscopic score of ulcerative colitis," *Therapeutic Advances in Gastroenterology*, vol. 16, 2023, doi: 10.1177/17562848231170945.

[21] K. Takenaka *et al.*, "Development and validation of a deep neural network for accurate evaluation of endoscopic images from patients with ulcerative colitis," *Gastroenterology*, vol. 158, no. 8, pp. 2150–2157, Jun. 2020, doi: 10.1053/j.gastro.2020.02.012.

[22] J. Maurício and I. Domingues, "Distinguishing between Crohn's disease and ulcerative colitis using deep learning models with interpretability," *Pattern Analysis and Applications*, vol. 27, no. 1, p. 1, Mar. 2024, doi: 10.1007/s10044-023-01206-3.

[23] R. W. Stidham *et al.*, "Using computer vision to improve endoscopic disease quantification in therapeutic clinical trials of ulcerative colitis," *Gastroenterology*, vol. 166, no. 1, pp. 155-167.e2, Jan. 2024, doi: 10.1053/j.gastro.2023.09.049.

[24] K. Gottlieb *et al.*, "Central reading of ulcerative colitis clinical trial videos using neural networks," *Gastroenterology*, vol. 160, no. 3, pp. 710-719.e2, Feb. 2021, doi: 10.1053/j.gastro.2020.10.024.

[25] S. Mohapatra, G. Kumar Pati, M. Mishra, and T. Swarnkar, "Gastrointestinal abnormality detection and classification using empirical wavelet transform and deep convolutional neural network from endoscopic images," *Ain Shams Engineering Journal*, vol. 14, no. 4, p. 101942, Apr. 2023, doi: 10.1016/j.asej.2022.101942.

[26] I. Iqbal, K. Walayat, M. U. Kakar, and J. Ma, "Automated identification of human gastrointestinal tract abnormalities based on deep convolutional neural network with endoscopic images," *Intelligent Systems with Applications*, vol. 16, p. 200149, Nov. 2022, doi: 10.1016/j.iswa.2022.200149.

[27] A. Mohammed, I. Farup, M. Pedersen, S. Yildirim, and Ø. Hovde, "PS-DeVCEM: pathology-sensitive deep learning model for video capsule endoscopy based on weakly labeled data," *Computer Vision and Image Understanding*, vol. 201, p. 103062, Dec. 2020, doi: 10.1016/j.cviu.2020.103062.

[28] J. Pei *et al.*, "Utility of four machine learning approaches for identifying ulcerative colitis and Crohn's disease," *Heliyon*, vol. 10, no. 1, p. e23439, Jan. 2024, doi: 10.1016/j.heliyon.2023.e23439.

[29] X. Jiang, X. Luo, Q. Nan, Y. Ye, Y. Miao, and J. Miao, "Application of deep learning in the diagnosis and evaluation of ulcerative colitis disease severity," *Therapeutic Advances in Gastroenterology*, vol. 16, Jan. 2023, doi: 10.1177/17562848231215579.

[30] M. Chierici *et al.*, "Automatically detecting Crohn's disease and Ulcerative Colitis from endoscopic imaging," *BMC Medical Informatics and Decision Making*, vol. 22, no. S6, p. 300, Nov. 2022, doi: 10.1186/s12911-022-02043-w.

BIOGRAPHIES OF AUTHORS

S. Bhuvaneswari is an assistant professor at cardamom planters' association college, Affiliated by Madurai kamaraj university, Madurai. She pursued Master of science in computer science from Madurai kamaraj university.she holds an M.Phil. degree in Computer Science with specialization in Datamining.Her research interest includes image/signal processing, medical image analysis DL., Datascience, AInce. She can be contacted at email: bhuvaneswari.s@cpacollege.org.

Dr. M. Sulthan ibrahim is an associate professor and head of the Department in Department of Computer Science, Government Arts and Science College, Veerapandi, Theni, Tamil Nadu, India since June 2016. He pursed Master of Philosophy in Computer Science from madurai kamaraj university, India in 2004 and Doctor of Philosophy from Bharathidhasan University in year 2016. His main research work focuses on data mining, web mining, cryptography and network security, IoT and AI based education. He has published Research paper in various International Journals and Conferences. He serves as doctral committee members of the varios univeristites. He has 25 years of teaching experience and more than 16 years of Research Experience. He can be contacted at email: km.sulthan@gmail.com.